Paul R. Medwell and Bassam B. Dally
Effect of fuel composition on jet flames in a heated and diluted oxidant stream
Combustion and Flame, 2012; 159(10):3138-3145

Published at: http://dx.doi.org/10.1016/j.combustflame.2012.04.012

Full-length article:

Effect of fuel composition on jet flames in a heated and diluted oxidant stream

Paul R. Medwell *, Bassam B. Dally

School of Mechanical Engineering, The University of Adelaide, S.A. 5005 Australia

Abstract

The role of hydrogen addition on the structure of the Moderate or Intense Low oxygen Dilution (MILD) combustion regime is examined using a combination of experimental techniques and laminar flame calculations. Laser diagnostic imaging is used to simultaneously reveal the in-situ distribution of the hydroxyl radical (OH), formaldehyde (H_2CO), and temperature using the Jet in Hot Coflow (JHC) burner. The fuels considered are natural gas, ethylene, and LPG (each diluted with hydrogen 1:1 by volume). Hydrogen addition to the primary fuel was found necessary to stabilise the flames. Further to the role of hydrogen in the stabilisation of the flames, hydrogen addition also leads to the reaction zone exhibiting similar structure for different primary fuel types. The independence of the reaction zone structure with hydrogen addition suggests that a wide variety of fuels may be usable for achieving MILD combustion.

* Corresponding Author. Tel: +61 (0)8 8303 5460; Fax: +61 (0)8 8303 4367
Email address: paul.medwell@adelaide.edu.au (Paul R. Medwell).

1 Introduction

The combustion of fuel in a heated and diluted oxidant stream results in a unique combustion regime referred to as Moderate or Intense Low oxygen Dilution (MILD) combustion [1]. The strong recirculation of exhaust gases back into the reaction zone results in a localised reduction in O_2 level, leading to a distributed reaction zone. The result of MILD combustion is a reduction in pollutant emissions (notably NO_x) and an increase in net radiation flux [2, 3]. Application of MILD combustion has been successfully applied in numerous applications, additionally incorporating the use of biomass fuel [4]. MILD combustion is typified by low (near unity) Damköhler numbers [5], and has the potential for cost effective low NO_x gas turbine power generation [6].

The depleted O_2 oxidant at elevated temperatures, necessary for MILD combustion, is typically realised by the recirculation of hot exhaust gases. Recirculation may be achieved either internally or externally with regard to the combustor. The complex interactions within such a system make it unsuitable for a fundamental study of the reaction zone. Instead, in this study an experimental burner is used to emulate MILD combustion under controlled conditions. The Jet in Hot Coflow (JHC) burner [7] enables a range of combustion parameters to be varied independently, and decouples the flow from the chemical kinetics. The JHC burner has been used for both experiments [7–10] and modelling [11–19]. A similar burner has also been used for combined experiments [20, 21] and modelling [22].

Despite much progress in the application of MILD combustion to practical systems, there remain unresolved issues on the stabilisation, auto-ignition,

and structure of the reaction zone near the jet exit under the hot and diluted conditions [10, 23, 24]. In particular, the influence of fuel type on the fundamental aspects of the combustion remain poorly understood. From a global perspective, MILD combustion features have been shown to be insensitive to fuel type, including liquid fuels [25]. Similarly, in a furnace environment it has been observed that the combustion of light fuel oil is very similar to natural gas, though differences were observed for heavy fuel oil and coal [26]. Furthermore, MILD combustion is particularly well-suited to using low calorific value (LCV) fuels [27]. Notably, the operation of a furnace using natural gas and biogas (60% CH_4 / 40% CO_2) has shown similar performance and emissions [28], as shown elsewhere [29]. MILD combustion has been demonstrated for both LCV fuels and industrial waste in the presence of hydrogen [30], with coke oven gas [31, 32], and in gas turbine combustors with LCV fuels [33]. There is also a move toward using coal with MILD combustion [34, 35]. Nonetheless, detailed fundamental understanding of MILD combustion of non-conventional fuels has yet to be widely achieved [31]. While other studies have used both methane and propane for MILD combustion [36], the present paper aims to provide a dedicated detailed fundamental-level investigation on the effect of fuel composition.

Hydrogen has been proposed as a "clean fuel" alternative for the future, in particular for use as a supplemental fuel additive [37, 38]. Whilst the use of pure hydrogen eliminates CO_2 emissions, it requires a redesign of existing burners [18]. Avoiding the need for purity, hydrogen may also be used for enrichment, which can be obtained using methods (such as gasification of biomass) that have both economical and environmental benefits [38]. The addition of hydrogen to other fuels is of particular interest to MILD combustion as it can

be well-controlled, improves the range of operating conditions and is also important for the incorporation of low calorific fuels [30]. Furthermore, although MILD combustion is effective at eliminating soot, the addition of hydrogen will further increase the ability to use fuels that have sooting tendencies [31].

Hydrogen is commonly used as a fuel enhancer to improve system reactivity, such as to promote ignition of low calorific value fuels [30]. The role of different hydrogen concentration with hydrocarbon (methane) fuel has been studied numerically by Mardani *et al.* [14], and shown to increase the reaction intensity. Hydrogen addition is known to improve laminar flame speed [39], and increase the maximum strain rate before extinction [40]. These features may enable operation over a wider range of conditions [30], but may require the redesign of conventional burners [38]. The addition of hydrogen increases the flame speed, such that flames are more likely to attach to the burner nozzle [38, 41, 42], which may negatively impact the operation of MILD combustion burners which require significant mixing of the fuel prior to reaction [31]. As expected, increased hydrogen concentration in the fuel also leads to increased OH concentration in the reaction zone [18, 38]. As a consequence of the reaction occurring closer to the exit, in conjunction with the higher reaction rates, there is less opportunity for the mixing that is required to achieve low-NO_x emissions [43]. Nonetheless, this effect will be dependent on burner configuration (especially burners that rely on entrainment due to high velocity). It has also been reported that NO_x emissions are not sensitive to the hydrogen concentration under MILD conditions [44], though this observation requires accurate understanding of NO formation via the NNH route [45]. Further details on NO_x formation are detailed in the literature [46–51]. It is important to note that relatively small quantities of hydrogen are required to

have significant changes on the combustion: further increasing the hydrogen concentration does not lead to proportional changes in the behaviour, which is attributed to the role of hydrogen in affecting the chain-branching [31], and highlights the importance of detailed chemistry in modelling such combustion [52]. The influential role of hydrogen addition has been observed to eliminate the region of "no ignition" in the jet stirred flow reactor of Sabia *et al.* [30].

In this paper the influence of combustion chemistry on the flame behaviour and reaction zone structure is examined by systematically increasing the fuel complexity under MILD combustion conditions. Temperature, the hydroxyl radical and formaldehyde are measured instantaneously and simultaneously using planar laser imaging techniques to reveal details of the structure of the reaction zone. The hydroxyl radical (OH) is used as a flame marker while the formaldehyde (H_2CO) intermediate species is predominant at low temperatures typical of those found in MILD combustion. The product of [OH] and [H_2CO] has also been suggested as an indicator of the formyl (HCO) radical, which is closely related to the heat release rate [53]. Three different fuels are considered, namely; natural gas (predominately methane), ethylene, and LPG (predominately propane). The difference in the chemical path for these fuel mixtures provides a way of assessing the sensitivity of the MILD combustion regime to fuel type (for gaseous hydrocarbon fuels). Each primary fuel is diluted with hydrogen (H_2) in an equal volumetric ratio to reduce the levels of soot and to stabilise the flame. The role of hydrogen addition is additionally investigated through laminar flame calculations. For each fuel type in the jet, differences in the fluid properties necessitates a change in the velocity to maintain the Reynolds number constant (at Re_{jet}=10,000) in order to maintain similar turbulence levels.

2 Experimental Details

The MILD combustion burner used in this study is the jet in hot coflow (JHC) burner used previously [8, 9], and shown in Figure 1. It consists of a central insulated fuel jet (⌀4.6mm) within an annular coflow (⌀82mm) of hot exhaust products from a premixed secondary burner mounted upstream of the jet exit plane. The coflow O_2 level is either 3% or 9% (volumetric), with an exit temperature of 1100K. Various hydrocarbon fuels are used in the jet; natural gas (NG), ethylene (C_2H_4) and liquefied petroleum gas (LPG). Each of these primary fuels is diluted with hydrogen (H_2) in an equal volumetric ratio. The addition of H_2 is found to be necessary to stabilise the flames. Hydrogen addition also lowers the level of soot, which is advantageous for laser measurements. Addition of H_2 also has implications for the potential use of hydrogen as a supplemental fuel additive. Noteworthy is that although the fuel stream is 50% H_2 by volume, it is less than 11% on a mass basis, and the heat release from the hydrogen is <25%. The jet Reynolds number for the experimental data presented in this paper is 10,000.

Laser induced fluorescence (LIF) is used to image OH and H_2CO, and temperature is inferred from Rayleigh scattering measurements. The laser pulses are fired sequentially to reduce interferences on the other systems, with the entire sequence occurring in 300ns to ensure the flow field is effectively frozen with respect to the fluid time scales. The in-plane resolution of all three ICCD cameras is 160µm, after spatial matching. The laser sheet heights were all ∼12mm, of which the central 8mm portion is presented herein. All images are corrected for laser power and profile variations shot-to-shot based on the signal from a laminar slot burner. Description of the experimental details is

described in-depth in a previous publication by the authors [8].

3 Laminar Flame Calculations

Laminar flame calculations have been performed to extend the study beyond the available measurements, and shed more light on the structure of the reaction zone and molecular transport. The OPPDIF routine of the Chemkin package is used to compute temperature and species concentration for opposed-flow diffusion flames. The opposed-flow laminar diffusion flame configuration represents a one-dimensional flame, analogous to the traverse across the well-defined reaction zone from fuel to oxidant. By increasing the velocity of the flow from two facing nozzles, the strain rate imposed on the flame front can be varied. The strain rate quoted throughout most of this paper is the average normal strain rate reported in the OPPDIF post-processor output. The use of a laminar, one-dimensional, configuration provided by the OPPDIF models is a well established methodology to enable the role of strain alone to be de-coupled from the more complex turbulent interactions that are observed experimentally [10]. Furthermore, it has previously been demonstrated that one-dimensional laminar diffusion flame calculations give excellent agreement with detailed single-point measurements in the JHC burner [7]. Other studies on the fundamental aspects of MILD combustion also have used this configuration [54, 55].

For all calculations the GRI-Mech 3.0 mechanism is used. Previous studies have shown the GRI mechanism to provide agreement with experimental measurements of the JHC burner used in this study under similar conditions [7, 12, 56]. Both thermal diffusion and multi-component diffusion models are

used for the calculations.

Since the coflow oxidant stream consists of combustion products (H_2O and CO_2), the standard definition of mixture fraction is not appropriately defined for calculations based on the mass fraction of H & C (hydrogen & carbon) atoms. A normalised mixture fraction, $\xi^* = (\xi - \xi_{oxi}) / (\xi_{fuel} - \xi_{oxi})$ is used instead, where ξ_{fuel} & ξ_{oxi} refer to the standard definition of mixture fraction at the fuel and oxidant stream boundaries, respectively.

4 Results

4.1 Visual Observations

Figure 2 shows photographs of the flames presented in this paper. The horizontal dashed lines at 35 & 125mm downstream of the jet exit plane indicate the locations of the laser diagnostic measurements. Apparent from Figure 2 is that the natural gas flames show significantly less soot than the ethylene and LPG flames. While soot is seen at both coflow O_2 levels for the ethylene and LPG flames, at the 3% O_2 level soot does not appear until around ∼200mm downstream, whereas for the 9% O_2 case soot appears much closer to the jet exit (∼100mm). For either fuel type, at the higher (9%) O_2 level, close to the jet exit the flame luminosity is significantly greater as compared to the lower (3%) O_2 case. The low luminosity of the 3% O_2 flames almost makes them appear invisible for the first ∼100mm. While not clearly apparent from the photographs, a faint reaction is indeed apparent in this region. Further downstream, once the effects of the coflow are diminished by the entrainment of surrounding air (*viz.* ∼100mm), soot does begin to appear for either coflow

O_2 level. The presence of soot around the 125mm downstream location in the 9% O_2 flames could potentially interfere with laser diagnostic measurements, and so data is collected at this location for the 3% O_2 flames only.

4.2 Typical Features

Figure 3 presents typical image triplets of OH, H_2CO and temperature for each flame condition (three fuel types, each at two coflow O_2 levels). The measurements are centred at 35mm downstream of the jet exit plane. The corresponding size of each image is 8mm in height and 35mm wide. The jet centreline is marked by the vertical dashed line. These images are for a jet Reynolds number of 10,000 and are typical of other Reynolds number flames as well. Despite the flow being nominally turbulent, the majority of the images show no sign of large-scale turbulent structure.

In each of the images presented in Figure 3 the OH appears as an unconvoluted layer which is quite uniform in intensity along the length of the sheet. For each fuel type, the OH concentration is considerably less at 3% O_2 as compared to the 9% O_2 case. The suppression of OH with a reduction in O_2 level is consistent with previous work (*e.g.* [8, 57]) and is directly related to the reduced temperature of the reaction zone. At either O_2 level the OH concentration does not significantly vary with the fuel type.

The temperature in the coflow is seen to be uniform. With the 9% O_2 coflow the temperature is seen to increase in the region corresponding to OH. For all of the 3% O_2 cases there is no obvious sign of a temperature increase across the reaction zone, although a reaction is clearly taking place as identified by

198 the presence of OH. Similar observations regarding the very low, almost in-
199 distinguishable temperature rise across the reaction zone has been seen in a
200 MILD combustion furnace [58]. The low measured temperatures are believed
201 to be genuine, and not because of interferences or problems with the Rayleigh
202 to temperature conversion process. Noteworthy is that the laser-based mea-
203 surements of the jet and coflow temperatures agree well with those expected,
204 and were also confirmed with thermocouple measurements.

205 The H_2CO concentration varies with both the O_2 level and even more dra-
206 matically with the type of fuel. Most notably, the 3% O_2 C_2H_4/H_2 flame has
207 significantly higher H_2CO than any other flame. In all cases the H_2CO appears
208 quite uniformly distributed and always exists on the fuel-rich side of the OH
209 layer. The broad radial distribution of H_2CO is also seen in strained laminar
210 flame calculations [9].

211 *4.3 Radial Profiles*

212 Figure 4 shows the mean and RMS radial profiles of OH, H_2CO, and tem-
213 perature for both 3% and 9% O_2 for the various fuel types, and at an axial
214 location 35mm above the jet exit plane. Each plot is generated only from the
215 central 3mm strip of the images, and not from the entire sheet height, so as to
216 avoid potentially over-corrected values towards the edge of the images where
217 the low laser energy possibly makes sheet corrections less reliable.

218 The instantaneous images presented (Figure 3) suggest that each of the vari-
219 ous fuel types have a very similar structure. This is also seen in the radial plots
220 of Figure 4. At the 3% O_2 coflow the mean OH profiles seem quite coincident,

with each fuel having a similar peak mean value and similar spatial shape. These observations are consistent with the similarity of global features observed in a MILD combustion reactor [25]. Nonetheless, in both the mean and RMS, there is a slight shift of the OH profiles inward towards the centreline as the fuel complexity is increased. This radial shift corresponds to a drop in jet velocity required to maintain the jet Reynolds number. At the 9% O_2 coflow the radial shift of the OH peak with the fuel type is more noticeable. Also more noticeable for the 9% case is a variation in the mean OH peak, although the changes are still relatively small. Worth noting is that despite an almost three-fold difference in the jet exit velocity for the various fuels, because the Reynolds number is constant in all cases, the OH RMS is comparable for either O_2 level.

At both coflow O_2 levels, in the H_2CO profiles of Figure 4 a very significant increase is noted for the C_2H_4/H_2 flame. The mean H_2CO is distributed widely across the radial profiles, but does show evidence of a dip along the jet centreline. The broad radial distribution of H_2CO has already been noted in the instantaneous images, and is consistent with strained laminar flame calculations. The H_2CO levels in the C_2H_4/H_2 flame are significantly higher with the 3% O_2 coflow as compared to 9% O_2, but for the other fuels (natural gas/H_2 & LPG/H_2) the H_2CO is similar at either O_2 level.

As was noted in the instantaneous images, the temperature rise across the reaction zone in the 3% O_2 coflow is barely discernible. For the 3% O_2 LPG/H_2 flame the temperature rise is not resolved in the mean profile. The lack of temperature rise has already been discussed in the typical instantaneous images. It is also important to note that the fluctuations in the radial location cause the peak in the mean radial profile to be significantly lower than instanta-

neous temperature peak. The low temperature rise in the mean radial profiles is consistent with previous single-point data measured in the JHC burner under MILD conditions [7]. At the 9% O_2 coflow, again the LPG/H_2 flame shows the lowest reaction zone temperature. The trends relating to the location of the peak temperature follows the same trend as seen in the OH profiles, *viz.* the peak shifts towards the centreline as the fuel complexity increases.

4.4 Laminar Flame Calculations

4.4.1 3% O_2 oxidant

The trends noted in the flame measurements can be compared to strained laminar flame calculations. It should be noted that due to the turbulent nature of the experimental measurements, the fluctuations in the reaction zone location will cause the mean OH and temperature measurements to be lower than those from laminar flame calculations. Figure 5 shows selected species concentrations in mixture fraction space for a strain rate of $\sim$100 s^{-1}. The temperature and OH, H_2CO & HCO mole fractions were obtained from OPPDIF calculations of the Chemkin package using GRI-Mech 3.0 mechanism. Previous studies have shown that the reaction structure is relatively insensitive to strain under MILD conditions, and that a strain rate of this order gives the best agreement with experimental measurements [7, 8]. A normalised mixture fraction (ξ^*) is used instead of the standard definition obtained from the calculations because of the non-standard oxidant stream composition [9]. The normalised mixture fraction ensures that ξ^* ranges from zero in the oxidant stream to one in the fuel stream. To observe features more clearly, the mixture fraction is only shown to 0.25, beyond which there are no features of interest.

Consistent with the measurements, the OH profiles in Figure 5 for the various fuels virtually overlap, both in location and peak value. There are some minor differences in the width of the OH profiles in Figure 5, but when normalised, the FWHM (full-width half-maximum) width varies by only around $\sim$5%. Similarly, the temperature profiles in Figure 5 across the reaction zone are also very similar, and virtually overlap for the different fuel types. At higher mixture fractions, the temperature for the CH_4/H_2 flame does roll-off a little faster than the others, but the differences are relatively minor. The general observations regarding OH and temperature confirm the experimental result that the fuel type has only minor effects on the reaction zone structure.

While the OH and temperature do not seem to vary significantly with the type of fuel, from Figure 5, H_2CO does show very different behaviour depending on the fuel type. In all cases, H_2CO is found almost over the entire range of mixture fraction, extending well beyond the presented range. This explains the very wide radial distribution of H_2CO in the images and reinforces that PAH or Raman interference is not responsible for the distribution seen in the measurements. It is therefore more appropriate to make comparisons away from the stoichiometric conditions. It is only for the CH_4/H_2 flame that the H_2CO peak is located near the stoichiometric mixture fraction. Both the C_2H_4/H_2 and C_3H_8/H_2 flames reach a local maximum around stoichiometry, but further toward the fuel rich side the H_2CO concentration dips slightly and then increases again. Analysis of the H_2CO rate of production indicates that the $C_2H_3+O_2 \rightleftharpoons HCO+H_2CO$ reaction is primarily responsible for the presence of of H_2CO in the fuel rich region. In this region, the concentration of C_2H_3 is higher in the C_2H_4/H_2 and C_3H_8/H_2 flames, leading to the higher concentration of H_2CO. The localised dip in H_2CO between stoichiometry and the fuel

rich region is a result of the increased H_2CO consumption via the $H+H_2CO \rightleftharpoons HCO+H_2$ reaction.

Also plotted in Figure 5 is the HCO mole fraction. As expected, HCO lies in between the OH and H_2CO profiles. The HCO profile does change somewhat with the fuel type. For CH_4/H_2 the HCO is narrower but has a higher peak, whereas C_2H_4/H_2 and C_3H_8/H_2 are more spread out, but only slightly more so.

Noteworthy is that the peak temperature measured is lower than the laminar flame calculations. This is not fully understood, though the effect of radiation which is not accounted for in the calculations may be a contributing factor, along with some uncertainty in resolving the Rayleigh cross-section across the reaction zone. Significantly, the experimental results correctly capture the coflow and jet temperatures.

4.4.2 9% O_2 oxidant

For the 9% O_2 coflow case, Figure 6 shows the same profiles as Figure 5. The temperature, OH and HCO all seem to have a similar response to the fuel type as already noted for the 3% O_2 case. Consistent with the measurements, the location of the OH peak again does not seem to be highly dependent on the fuel type, and the peak concentration is also relatively constant. At 9% O_2 the differences between the different fuels are somewhat more pronounced, but the general trends and observations are comparable.

At 9% O_2 the H_2CO distribution is again seen to be wide, extending well into the fuel rich side. Unlike at 3% O_2, at 9% O_2 the H_2CO profiles do not

change quite as significantly with fuel type, although the differences are still noticeable. The basic profile for each of the fuels is somewhat consistent, with a peak just to the rich side of stoichiometry and a long tail extending further to the fuel rich side. Noteworthy is that unlike the 3% O_2 oxidant, the H_2CO does not increase in the fuel rich region for the 9% O_2 case. This difference is a result of the reduced O_2 concentration in this region at 9% O_2, as compared with 3% O_2, inhibiting H_2CO formation via the $C_2H_3+O_2 \rightleftharpoons HCO+H_2CO$ reaction. The lower O_2 on the fuel rich side of the reaction zone at higher O_2 oxidant stream concentration has been discussed previously [10].

The stoichiometric mixture fraction, as indicated by the HCO peak, is seen to shift between the different fuels more for 9% O_2 than for 3% O_2. This shift in stoichiometry becomes more noticeable as the stoichiometric mixture fraction becomes larger, but is still relatively small.

4.4.3 21% O_2 oxidant

To compare the similarity of the reaction zone structure for the different fuels under the hot and diluted O_2 conditions, strained laminar flame calculation results are shown for standard air (21% O_2, 300K) in Figure 7. Apparent is that unlike for the MILD combustion conditions, the fuel type does lead to clear differences in the species profiles. While the OH profiles remain similar, in comparison to the 3% and 9% O_2, 1100K temperature oxidant stream case, the OH profiles are no longer coincident. This suggests that the MILD combustion conditions are fundamentally responsible for bringing about the similarity of the temperature and OH profiles for the different fuels.

4.4.4 Effect of hydrogen addition

The comparison between the three different gaseous hydrocarbon fuels presented thus far has revealed that the fuel type does not have a significant effect on the reaction zone structure under MILD combustion conditions. It is important to highlight that each of the primary fuels were diluted with hydrogen (H_2) in equal volumetric parts. The addition of H_2 was necessary to increase the flame stability to prevent blow-off. Hydrogen also shifts the stoichiometric mixture fraction to the lean side, towards the edge of the shear layer. The H_2 added to the fuel stream seems to influence the kinetics such that the different hydrocarbon fuels show similar characteristics.

It was found from experimentation that when H_2 was not added to the jet the flames would typically blow-off. Only the C_2H_4 flame could be sustained, and even then, it appeared lifted. The importance of H_2 addition to the fuel is also reflected in laminar flame calculations. For the experimental 3% O_2 oxidant stream conditions, calculations show no temperature rise across the reaction zone for the pure fuels without H_2 in the fuel stream, except at a very low strain rate. These trends in the calculation for the undiluted fuel types are in agreement with those noted during the experiments with the JHC burner. These results also highlight the importance of H_2 to ignition, and thus the importance of hydrogen-enrichment in the context of practical applications.

To examine the structural differences without H_2 addition to the fuel, Figure 8 shows selected species concentrations found from strained laminar flame calculations. The conditions for Figure 8 are identical as for the previously presented Figure 6, but without H_2 added to the fuel. As outlined in the preceding paragraph, comparisons can only be made at the 9% O_2 case, as at the

3% O_2 conditions a reaction could not be sustained.

Comparison of Figure 8 (no H_2 addition) to Figure 6 (with H_2 addition) reveals major differences in the selected species concentrations. Unlike with H_2 diluted fuels, Figure 8 shows that the OH profiles are dependent on the fuel type. For C_2H_4, the peak OH concentration is 30% higher, and the FWHM (full-width half-maximum, in the normalised mixture fraction space) is 40% wider, than for CH_4 fuel. Significant differences for the various fuel types in the H_2CO and HCO profiles are also far more pronounced than seen with H_2 addition. Comparison of the peak concentration in the reaction zone of H_2CO and HCO reveals that both increase by approximately a factor of 3.5 without H_2 addition.

The role of H_2 leading to a similar reaction zone structure is important for the use of low calorific value fuels. These results suggest that H_2 not only improves reactivity but also changes the structure of the reaction zone.

5 Discussion

From the instantaneous images and the radial profiles that have been presented there does not seem to be any significant effect of the fuel type on the structure of the reaction zone. Similar trends are also observed at other measurement locations. The trends obtained from methane and propane fuels have previously been noted as being similar in a heated and diluted oxidant stream in a spectral emission study [59], and are consistent with the similar global behaviour reported previously [25, 26, 28, 29].

Of the measured scalars, the H_2CO number density changes the most between

the different fuel types considered. Nonetheless, the basic behaviour of the H_2CO is essentially constant between the different fuel cases. Changes in the flow structure are also apparent for the different fuel types. These differences arise because of the different jet velocity for each fuel type (required to maintain constant Reynolds number). Despite these minor differences, the fuel type does not lead to any major changes in the overall flame characteristics at the measurement locations under MILD conditions.

The photographs of the flames (Figure 2) provide supplemental evidence supporting the similarity of the different fuel types when in the confines of the hot and diluted coflow. Further downstream, after the effects of the coflow have diminished, each of the flames visually appear significantly different. This is suggestive of the importance of the coflow in establishment of the unique conditions which lead to the similarity between the different fuels.

Table 1 shows the average of the peak OH values in each of the images for a particular flame. Also included is the standard deviation (as a percentage) of the values. In determining the peak value in each of the images, only the central 3mm portion of the image is included to avoid over-corrected values towards the edges of the images where the low laser power makes sheet corrections less reliable. Table 1 reiterates the similarity of the OH levels for the different fuel compositions. At either O_2 level the mean peak OH number density is very similar for each fuel. Consistent with the radial profiles, the similarity is especially noted for the 3% O_2 case.

At the 35mm location, where the oxidant composition is well defined and not yet affected by surrounding air entrainment, comparisons of the trends can be made to the strained laminar flame calculations. Table 2 presents the peak

temperature, and the maximum number density of OH and H_2CO for each fuel type and at both O_2 levels obtained from the OPPDIF calculations.

Comparing Tables 1 & 2 it is seen that calculations support the measurements, in that the OH concentration does not change significantly with the fuel composition. The experimental peak OH value for the 3% O_2 flames is higher than from the calculations, whereas at 9% O_2 the calculated value is higher than that found from the experiment. The typical differences between the measured value and calculations is approximately 25% for 3% O_2 and ~40% for 9% O_2. Nevertheless, there is good similarity of the trends, and also a similar order of magnitude between the experiments and calculations.

Table 2 shows that the H_2CO in the C_2H_4/H_2 flame behaves the opposite to the other two fuels. For C_2H_4/H_2 the H_2CO significantly increases at the lower O_2 case. In contrast, the effect of O_2 on H_2CO is comparatively minor for the other fuels. For C_3H_8/H_2 there is little difference between the two O_2 levels. In the CH_4/H_2 flame the trend is reversed and H_2CO slightly increases with O_2 level. The different behaviour of the H_2CO in the C_2H_4/H_2 flames to the other fuels was also apparent in the experimental data presented. Of particular note in the C_2H_4/H_2 flames was that the H_2CO levels in the 3% O_2 flames was much higher than the other cases, which is consistent with the laminar flame calculations (Table 2). At 9% O_2, Table 2 indicates that the C_2H_4/H_2 flame should have lower H_2CO than the other flames, which is not seen in the experimental data. Nevertheless, in general, the trends of H_2CO largely follow those predicted by the flame calculations shown in Table 2.

It is important to highlight that each of the primary fuels are diluted with hydrogen (H_2) in equal volumetric parts. The addition of H_2 is necessary to

increase the flame stability to prevent blow-off. The H_2 added to the fuel stream seems to influence the kinetics such that the different hydrocarbon fuels show similar characteristics.

6 Conclusions

The comparison between the three different gaseous hydrocarbon fuels in this paper reveals that the fuel type does not have a significant effect on the reaction zone structure under MILD combustion conditions, when mixed with hydrogen. The primary fuels considered were natural gas, ethylene, and LPG (each diluted with H_2 1:1 by volume). Both experimental measurements and strained laminar flame calculations indicate that the reaction zone structure is very similar for the different fuels considered when hydrogen is added to the fuel stream. Hydrogen was found necessary for the experimental flames to stabilise. The OH concentration results were seen to be quite constant. Only minor changes of the OH spatial distribution were noted, and attributable to differences in fuel velocity required to maintain constant Reynolds number. The only significant changes with the fuel type were noted in the H_2CO levels, most notably with the C_2H_4/H_2 flame. The trends in the measured H_2CO levels were seen to be consistent with flame calculations. The similarity of the combustion characteristics for the various gaseous hydrocarbon fuels considered suggests that MILD combustion should be readily adapted for different fuel types. The insensitivity to fuel type is potentially a significant advantage for the implementation and application of MILD combustion to practical systems.

Acknowledgments

The authors would like to thank Dr Peter Kalt and Dr Zeyad Alwahabi for their assistance with this project. The financial support of The University of Adelaide and the Australian Research Council is gratefully acknowledged.

References

[1] A. Cavaliere, M. de Joannon, Mild combustion, Progress in Energy and Combustion Science 30 (2004) 329–366.

[2] G.-M. Choi, M. Katuski, Advanced low NO_x combustion using highly preheated air, Energy Conversion and Management 42 (2001) 639–652.

[3] R. Weber, S. Orsino, N. Lallemant, A. Verlaan, Combustion of natural gas with high-temperature air and large quantities of flue gas, Proceedings of the Combustion Institute 28 (2000) 1315–1321.

[4] 8^{th} International Symposium of High Temperature Air Combustion and Gasification, Poznań, Poland, 2010.

[5] C. Galletti, A. Parente, L. Tognotti, Numerical and experimental investigation of a mild combustion burner, Combustion and Flame 151 (2007) 649–664.

[6] Y. D. Wang, Y. Huang, D. McIlveen-Wright, J. McMullan, N. Hewitt, P. Eames, S. Rezvani, A techno-economic analysis of the application of continuous staged-combustion and flameless oxidation to the combustor design in gas turbines, Fuel Processing Technology 87 (2006) 727–736.

[7] B. B. Dally, A. N. Karpetis, R. S. Barlow, Structure of turbulent non-premixed jet flames in a diluted hot coflow, Proceedings of the Combustion Institute 29 (2002) 1147–1154.

[8] P. R. Medwell, P. A. M. Kalt, B. B. Dally, Simultaneous imaging of OH, formaldehyde, and temperature of turbulent nonpremixed jet flames in a heated and diluted coflow, Combustion and Flame 148 (2007) 48–61.

[9] P. R. Medwell, P. A. M. Kalt, B. B. Dally, Imaging of diluted turbulent ethylene flames stabilized on a Jet in Hot Coflow (JHC) burner, Combustion and Flame 152 (2008) 100–113.

[10] P. R. Medwell, P. A. M. Kalt, B. B. Dally, Reaction zone weakening effects under hot and diluted oxidant stream conditions, Combustion Science and Technology 181 (7) (2009) 937–953.

[11] S. H. Kim, K. Y. Huh, B. Dally, Conditional moment closure modeling of turbulent nonpremixed combustion in diluted hot coflow, Proceedings of the Combustion Institute 30 (2005) 751–757.

[12] F. C. Christo, B. B. Dally, Modeling turbulent reacting jets issuing into a hot and diluted coflow, Combustion and Flame 142 (2005) 117–129.

[13] J. Aminian, C. Galletti, S. Shahhosseini, L. Tognotti, Key modeling issues in prediction of minor species in diluted-preheated combustion conditions, Applied Thermal Engineering 31 (2011) 3287–3300.

[14] A. Mardani, S. Tabejamaat, Effect of hydrogen on hydrogen-methane turbulent non-premixed flame under mild condition, International Journal of Hydrogen Energy 35 (2010) 11324–11331.

[15] A. Mardani, S. Tabejamaat, M. Ghamari, Numerical study of influence of molecular diffusion in the mild combustion regime, Combustion Theory and Modelling 14 (2010) 747–774.

[16] A. Frassoldati, P. Sharma, A. Cuoci, T. Faravelli, E. Ranzi, Kinetic and fluid dynamics modeling of methane/hydrogen jet flames in diluted coflow, Applied Thermal Engineering 30 (2010) 376–383.

[17] M. Ihme, Y. C. See, LES flamelet modeling of a three-stream MILD combustor: Analysis of flame sensitivity to scalar inflow conditions, Proceedings of the Combustion Institute 33 (2011) 1309–1317.

[18] F. Wang, J. Mi, P. Li, C. Zheng, Diffusion flame of a CH_4/H_2 jet in hot low-oxygen coflow, International Journal of Hydrogen Energy 36 (2011) 9267–9277.

[19] A. Parente, J. C. Sutherland, B. B. Dally, L. Tognotti, P. J. Smith, Investi-

gation of the MILD combustion regime via principal component analysis, Proceedings of the Combustion Institute 33 (2011) 3333–3341.

[20] E. Oldenhof, M. J. Tummer, E. H. van Veen, D. J. E. M. Roekaerts, Ignition kernel formation and lift-off behaviour of jet-in-hot-coflow flames, Combustion and Flame 157 (2010) 1167–1178.

[21] E. Oldenhof, M. J. Tummer, E. H. van Veen, D. J. E. M. Roekaerts, Role of entrainment in the stabilisation of jet-in-hot-coflow flames, Combustion and Flame 158 (2011) 1553–1563.

[22] A. De, E. Oldenhof, P. Sathiah, D. Roekaerts, Numerical simulation of Delft-Jet-in-Hot-Coflow (DJHC) flames using the eddy dissipation concept model for turbulence-chemistry interaction, Flow Turbulence Combust 87 (2011) 537–567.

[23] K. Maruta, K. Muso, K. Takeda, T. Niioka, Reaction zone structure in flameless combustion, Proceedings of the Combustion Institute 28 (2000) 2117–2123.

[24] M. de Joannon, A. Cavaliere, T. Faravelli, E. Ranzi, P. Sabia, A. Tregossi, Analysis of process parameters for steady operations in methane mild combustion technology, Proceedings of the Combustion Institute 30 (2005) 2605–2612.

[25] M. Derudi, R. Rota, Experimental study of the mild combustion of liquid hydrocarbons, Proceedings of the Combustion Institute 33 (2011) 3325–3332.

[26] R. Weber, J. P. Smart, W. vd Kamp, On the (MILD) combustion of gaseous, liquid, and solid fuels in high temperature preheated air, Proceedings of the Combustion Institute 30 (2005) 2623–2629.

[27] M. Mörtberg, W. Blasiak, A. K. Gupta, Combustion of normal and low calorific fuels in high temperature and oxygen deficient environment,

548 Combustion Science and Technology 178 (7) (2006) 1345–1372.
549 [28] A. F. Colorado, B. A. Herrera, A. A. Amell, Performance of a flameless
550 combustion furnace using biogas and natural gas, Bioresource Technology
551 101 (2010) 2443–2449.
552 [29] A. Effugi, D. Gelosa, M. Derudi, R. Rota, Mild combustion of methane-
553 derived fuel mixtures: natural gas and biogas, Combustion Science and
554 Technology 180 (2008) 481–493.
555 [30] P. Sabia, M. de Joannon, S. Fierro, A. Tregrossi, A. Cavaliere, Hydrogen-
556 enriched methane mild combustion in a well stirred reactor, Experimental
557 Thermal and Fluid Science 31 (2007) 469–475.
558 [31] M. Derudi, A. Villani, R. Rota, Sustainability of mild combustion of
559 hydrogen-containing hybrid fuels, Proceedings of the Combustion Insti-
560 tute 31 (2007) 3393–3400.
561 [32] M. Derudi, A. Villani, R. Rota, Mild combustion of industrial hydrogen-
562 containing byproducts, Industrial and Engineering Chemistry Research
563 46 (2007) 6806–6811.
564 [33] B. Danon, W. de Jong, D. J. E. M. Roekaerts, Experimental and nu-
565 merical investigation of a flox combustor firing low calorific value gases,
566 Combustion Science and Technology 182 (2010) 1261–1278.
567 [34] N. Schaffel, M. Mancini, A. Szlęk, R. Weber, Mathematical modeling of
568 mild combustion of pulverized coal, Combustion and Flame 156 (2009)
569 1771–1784.
570 [35] M. Vascellari, G. Cau, Influence of turbulence-chemical interaction on
571 cfd pulverized coal mild combustion modeling, Fuel (In press) (2011)
572 doi:10.1016/j.fuel.2011.07.042.
573 [36] M. Mörtberg, W. Blasiak, A. K. Gupta, Experimental investigation of
574 flow phenomena of a single fuel jet in cross-flow during highly preheated

air combustion conditions, Journal of Engineering for Gas Turbines and Power 129 (2007) 556–564.

[37] C. G. Fotache, T. G. Kreutz, C. K. Law, Ignition of hydrogen-enriched methane by heated air, Combustion and Flame 110 (1997) 429–440.

[38] A. Parente, C. Galletti, L. Tognotti, Effect of the combustion model and kinetic mechanism on the MILD combustion in an industrial burner fed with hydrogen enriched fuels, International Journal of Hydrogen Energy 33 (2008) 7553–7564.

[39] G. Yu, C. K. Law, C. K. Wu, Laminar flame speeds of hydrocarbon + air mixtures with hydrogen addition, Combustion and Flame 63 (1986) 339–347.

[40] G. S. Jackson, R. Sai, J. M. Plaia, C. M. Boggs, K. T. Kiger, Influence of H_2 on the response of lean premixed CH_4 flames to high strained flows, Combustion and Flame 132 (2003) 503–511.

[41] R. Lückerath, W. Meier, M. Aigner, FLOX® combustion at high pressure with different fuel compositions, Journal of Engineering for Gas Turbines and Power 130 (2008) 011505.

[42] A. Parente, C. Galletti, J. Riccardi, M. Schiavetti, L. Tognotti, Experimental and numerical investigation of a micro-CHP flameless unit, Applied Energy 89 (2012) 203–214.

[43] R. Sadanandan, R. Lückerath, W. Meier, C. Wahl, Flame characteristics and emissions in flameless combustion under gas turbine relevant conditions, Journal of Propulsion and Power 27 (5) (2011) 970–980.

[44] Y. Yu, W. Gaofeng, L. Qizhao, M. Chengbiao, X. Xianjun, Flameless combustion for hydrogen containing fuels, International Journal of Hydrogen Energy 35 (2010) 2694–2697.

[45] A. Parente, C. Galletti, L. Tognotti, A simplified approach for predicting

no formation in mild combustion of CH_4-H_2 mixtures, Proceedings of the Combustion Institute 33 (2011) 3343–3350.

[46] A. N. Hayhurst, E. M. Hutchinson, Evidence for a new way of producing NO via NNH in fuel-rich flames at atmospheric pressure, Combustion and Flame 114 (1998) 274–279.

[47] A. A. Konnov, G. Colson, J. De Ruyck, NO formation rates for hydrogen combustion in stirred reactors, Fuel 80 (2001) 49–65.

[48] G. J. Rørtveit, J. E. Hustad, S.-C. Li, F. A. Williams, Effects of diluents on NO_x formation in hydrogen counterflow flames, Combustion and Flame 130 (2002) 48–61.

[49] H. Guo, G. J. Smallwood, F. Liu, Y. Ju, Ö. L. Gülder, The effect of hydrogen addition on flammability limit and NO_x emission in ultra-lean couterflow CH_4/air premixed flames, Proceedings of the Combustion Institute 30 (2005) 303–311.

[50] P. Glarborg, M. U. Alzueta, K. Dam-Johansen, J. A. Miller, Kinetic modeling of hydrocarbon/nitric oxide interactions in a flow reactor, Combustion and Flame 115 (1998) 1–27.

[51] M. Skottene, K. E. Rian, A study of NO_x formation in hydrogen flames, International Journal of Hydrogen Energy 32 (2007) 3572–3585.

[52] C. Galletti, A. Parente, M. Derudi, R. Rota, L. Tognotti, Numerical and experimental analysis of NO emissions from a lab-scale burner fed with hydrogen-enriched fuels and operating in MILD combustion, International Journal of Hydrogen Energy 34 (2009) 8339–8351.

[53] H. N. Najm, P. H. Paul, C. J. Mueller, P. S. Wyckoff, On the adequacy of certain experimental observables as measurements of flame burning rate, Combustion and Flame 113 (1998) 312–332.

[54] M. de Joannon, P. Sabia, G. Sorrentino, A. Cavaliere, Numerical study

of mild combustion in hot diluted diffusion ignition (HDDI) regime, Proceedings of the Combustion Institute 32 (2009) 3147–3154.

[55] P. Sabia, M. de Joannon, G. Sorrentino, A. Cavaliere, Pyrolytic and oxidative structures in HDDI MILD combustion, International Journal on Energy for a Clean Environment 11 (2010) 21–34.

[56] S. H. Kim, K. Y. Huh, B. Dally, Conditional moment closure modeling of turbulent nonpremixed combustion in diluted hot coflow, Proceedings of the Combustion Institute 30 (2005) 751–757.

[57] T. Plessing, N. Peters, J. G. Wünning, Laseroptical investigation of highly preheated combustion with strong exhaust gas recirculation, Proceedings of the Combustion Institute 27 (1998) 3197–3204.

[58] I. B. Özdemir, N. Peters, Characteristics of the reaction zone in a combustor operating at MILD combustion, Experiments In Fluids 30 (2001) 683–695.

[59] T. Ishiguro, S. Tsuge, T. Furuhata, K. Kitagawa, N. Arai, T. Hasegaa, R. Tanaka, A. K. Gupta, Homogenization and stabilization during combustion of hydrocarbons with preheated air, Proceedings of the Combustion Institute 27 (1998) 3205–3213.

Fuel composition	Peak n_{OH} $[\sigma]$ ($\times 10^{16} cm^{-3}$)	
	3% O_2	9% O_2
NG/H_2	0.56 [11%]	1.28 [11%]
C_2H_4/H_2	0.56 [10%]	1.53 [30%]
LPG/H_2	0.54 [9%]	1.33 [8%]

Table 1
Mean and standard deviation (σ, in brackets) of peak OH number density measurements. Central 3mm strip of images used. Axial location 35mm above jet exit.

Fuel composition	Peak temp. (K)		Peak n_{OH} ($10^{16}cm^{-3}$)		Peak n_{H_2CO} ($10^{14}cm^{-3}$)	
	3%	9%	3%	9%	3%	9%
CH_4/H_2	1400	1876	0.40	2.04	1.15	1.93
C_2H_4/H_2	1403	1856	0.46	2.11	2.59	0.87
C_3H_8/H_2	1384	1807	0.43	1.97	1.60	1.45

Table 2
Peak temperature and OH & H_2CO number density (molecules/cm^3) from strained laminar flame calculations for 3% and 9% O_2 oxidant stream conditions ($a \approx 200 s^{-1}$).

List of Figure Captions

Figure 1: Cross-sectional diagram of jet in hot coflow (JHC) burner.

Figure 2: Photographs of natural gas (NG), ethylene (C_2H_4) & LPG flames, each diluted with hydrogen (1:1 vol/vol) at two coflow O_2 levels. Jet Reynolds number of 10,000. Note the different exposure times (all other camera parameters held constant). Horizontal lines indicate measurement locations (35mm & 125mm downstream of jet exit plane). Photograph height: 300mm.

Figure 3: Selection of instantaneous OH, H_2CO and temperature image triplets of natural gas/H_2, C_2H_4/H_2 and LPG/H_2 flames showing typical features. OH shown in number density (molecules/cm^3), H_2CO in arbitrary units, temperature in Kelvin. Re_{jet}=10,000. Each image 8×35mm. Jet centreline marked with dashed line. Axial location 35mm above jet exit.

Figure 4: Mean and RMS radial profiles of OH, H_2CO and temperature for natural gas/H_2, C_2H_4/H_2 and LPG/H_2 flames. OH shown in number density (molecules/cm^3), H_2CO in arbitrary units, temperature in Kelvin. Re_{jet}=10,000. Central 3mm strip of images used. Axial location 35mm above jet exit.

Figure 5: Temperature and species mole fractions from strained laminar flame calculations in (normalised) mixture fraction space for 3% O_2 coflow composition ($a \approx 100\text{s}^{-1}$).

Figure 6: Temperature and species mole fractions from strained laminar flame calculations in (normalised) mixture fraction space for 9% O_2 coflow composition ($a \approx 100\text{s}^{-1}$).

Figure 7: Temperature and species mole fractions from strained laminar flame calculations in (normalised) mixture fraction space for (21% O_2, 300K) air

($a \approx 100\text{s}^{-1}$).

Figure 8: Temperature and species mole fractions from strained laminar flame calculations in (normalised) mixture fraction space for 9% O_2 coflow composition ($a \approx 100\text{s}^{-1}$).

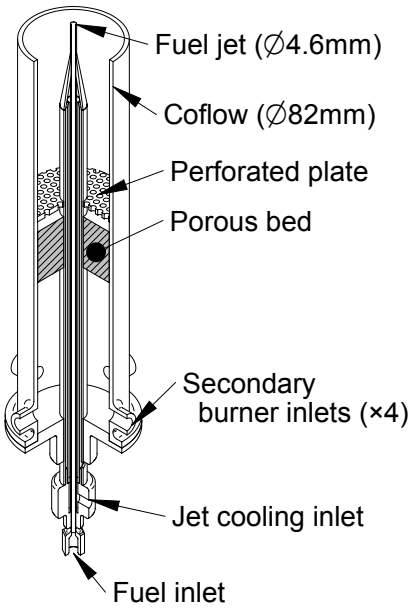

Fig. 1. Cross-sectional diagram of jet in hot coflow (JHC) burner.

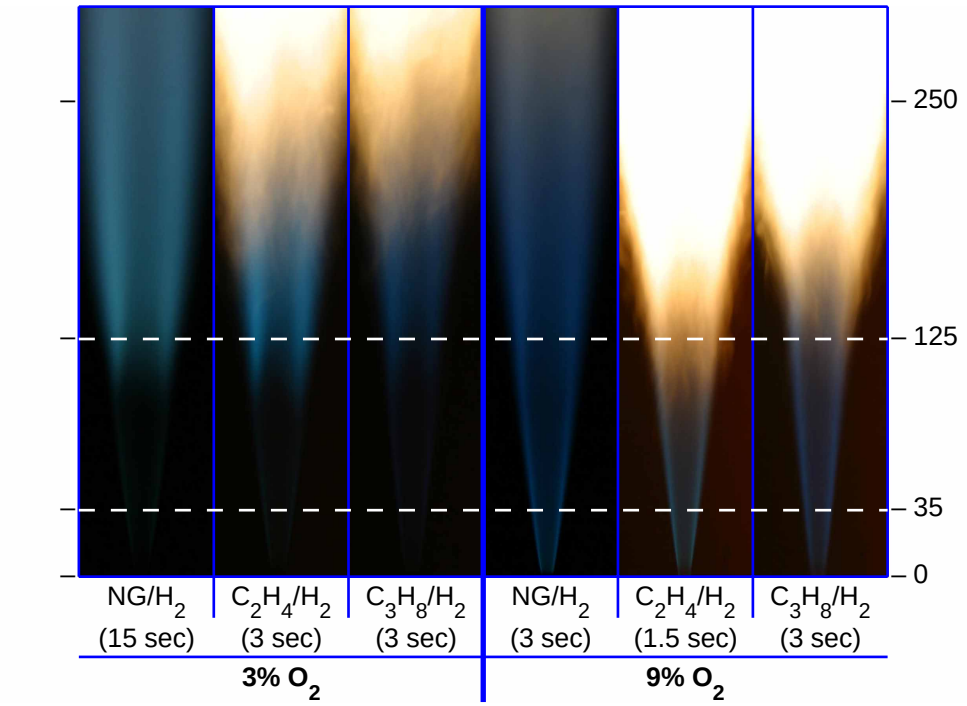

Fig. 2. Photographs of natural gas (NG), ethylene (C_2H_4) & LPG flames, each diluted with hydrogen (1:1 vol/vol) at two coflow O_2 levels. Jet Reynolds number of 10,000. Note the different exposure times (all other camera parameters held constant). Horizontal lines indicate measurement locations (35mm & 125mm downstream of jet exit plane). Photograph height: 300mm.

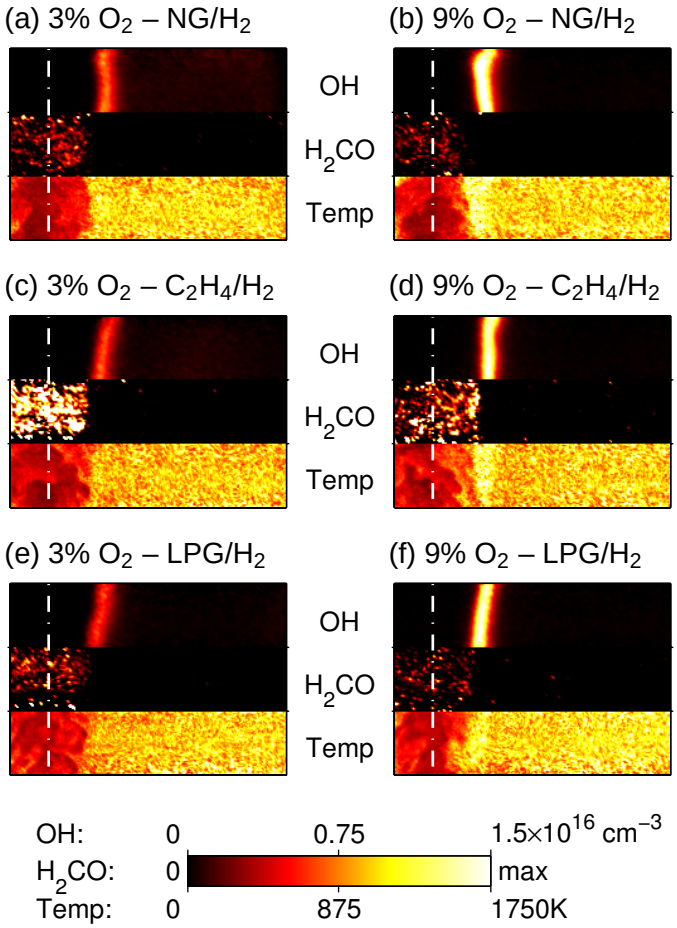

Fig. 3. Selection of instantaneous OH, H_2CO and temperature image triplets of natural gas/H_2, C_2H_4/H_2 and LPG/H_2 flames showing typical features. OH shown in number density (molecules/cm^3), H_2CO in arbitrary units, temperature in Kelvin. Re_{jet}=10,000. Each image 8×35mm. Jet centreline marked with dashed line. Axial location 35mm above jet exit.

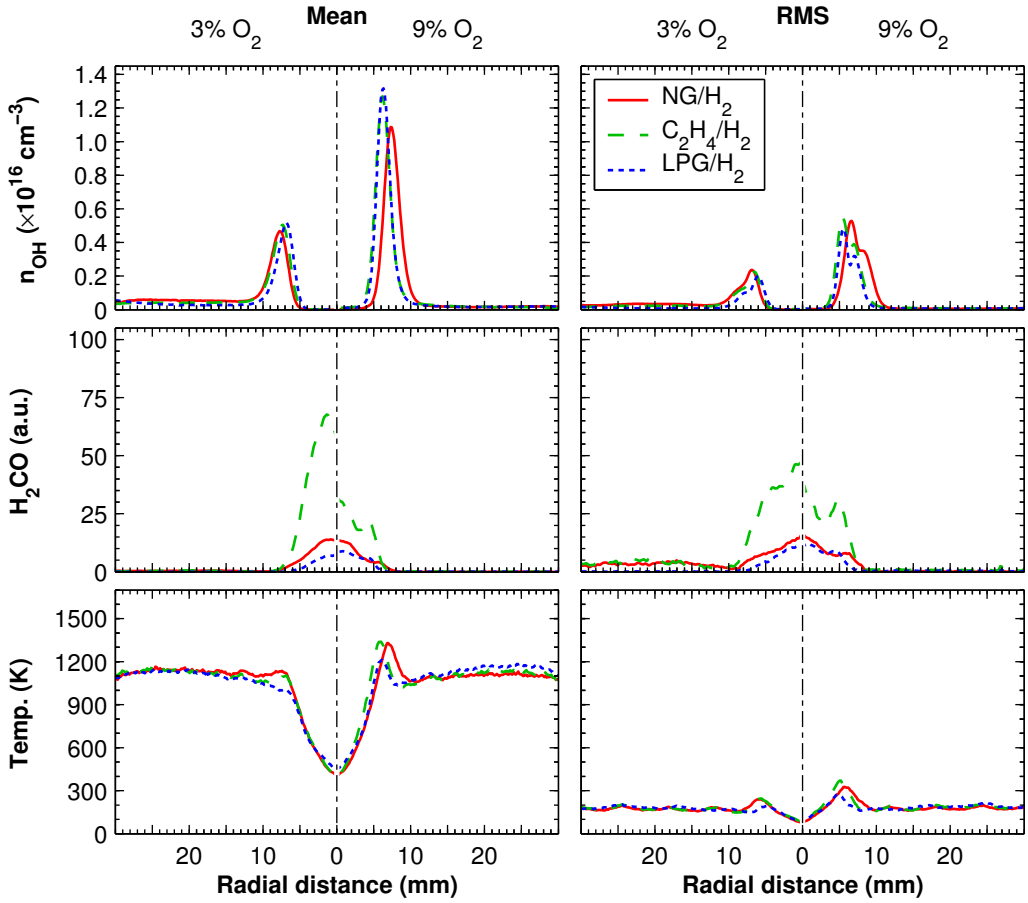

Fig. 4. Mean and RMS radial profiles of OH, H_2CO and temperature for natural gas/H_2, C_2H_4/H_2 and LPG/H_2 flames. OH shown in number density (molecules/cm^3), H_2CO in arbitrary units, temperature in Kelvin. Re_{jet}=10,000. Central 3mm strip of images used. Axial location 35mm above jet exit.

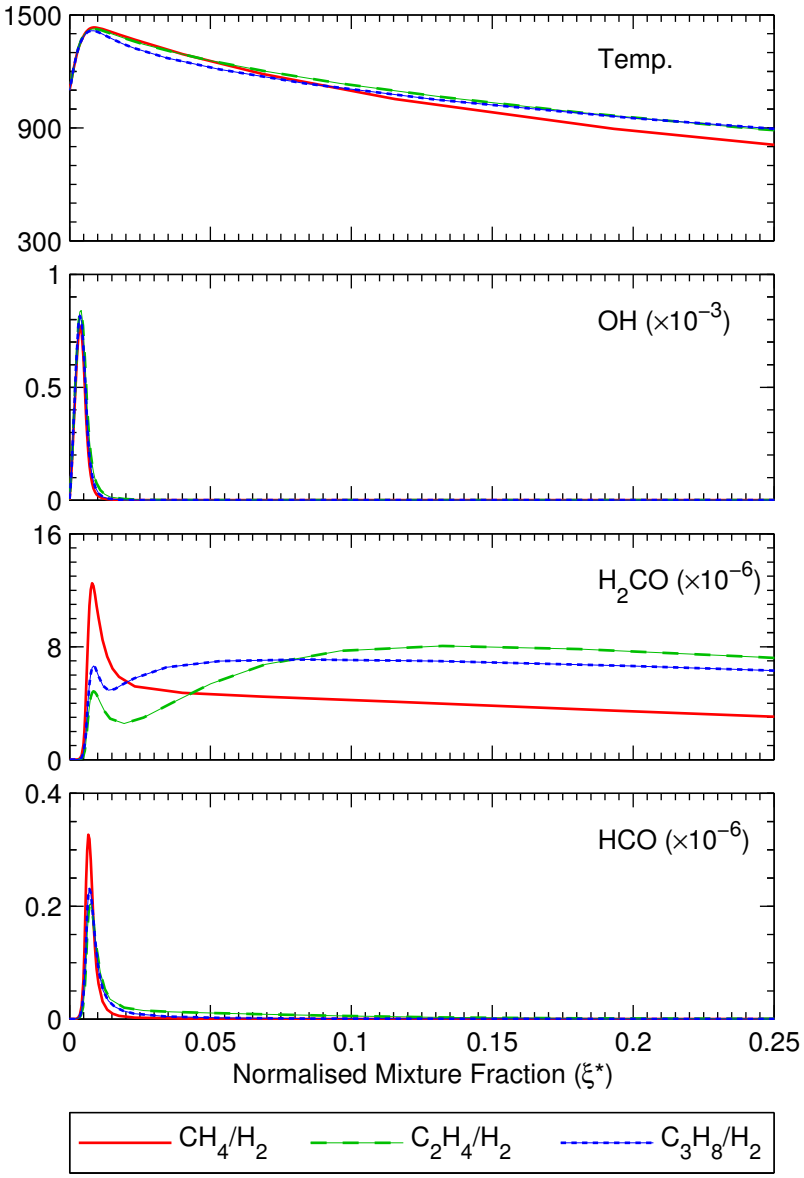

Fig. 5. Temperature and species mole fractions from strained laminar flame calculations in (normalised) mixture fraction space for 3% O_2 coflow composition ($a \approx 100 s^{-1}$).

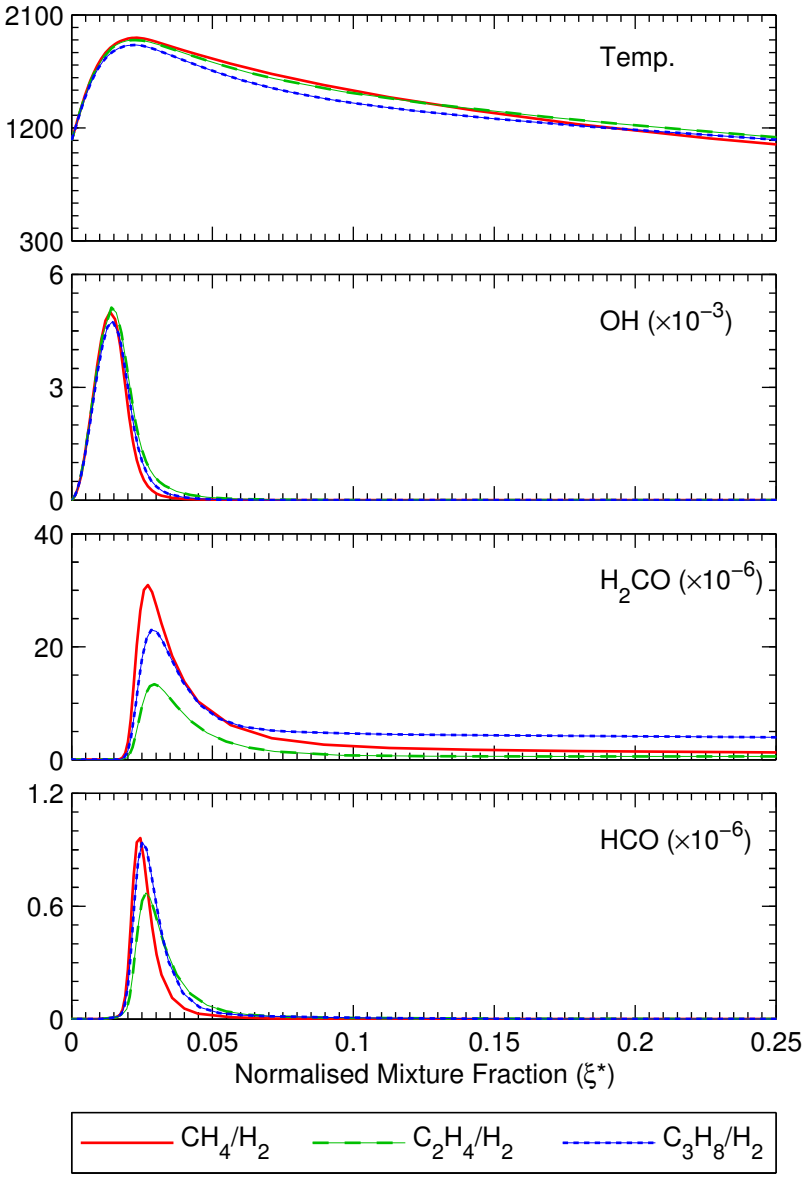

Fig. 6. Temperature and species mole fractions from strained laminar flame calculations in (normalised) mixture fraction space for 9% O_2 coflow composition ($a \approx 100 s^{-1}$).

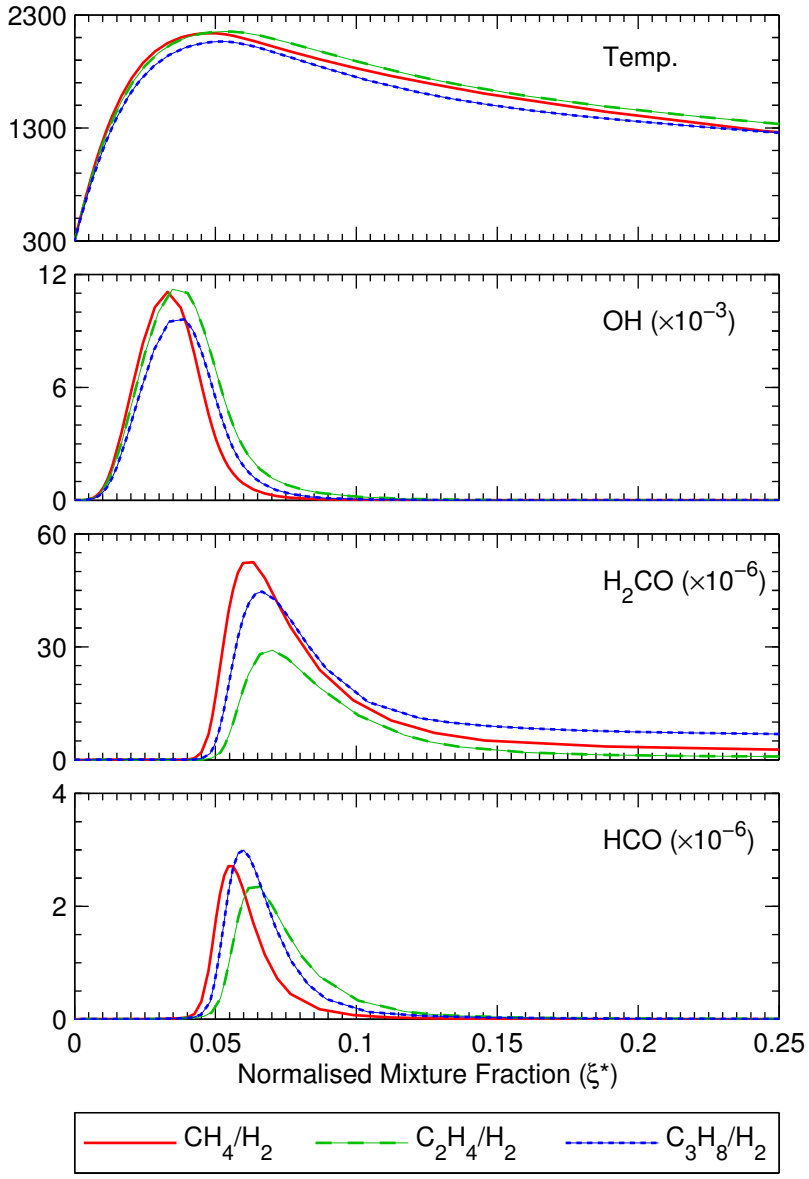

Fig. 7. Temperature and species mole fractions from strained laminar flame calculations in (normalised) mixture fraction space for (21% O_2, 300K) air ($a \approx 100 s^{-1}$).

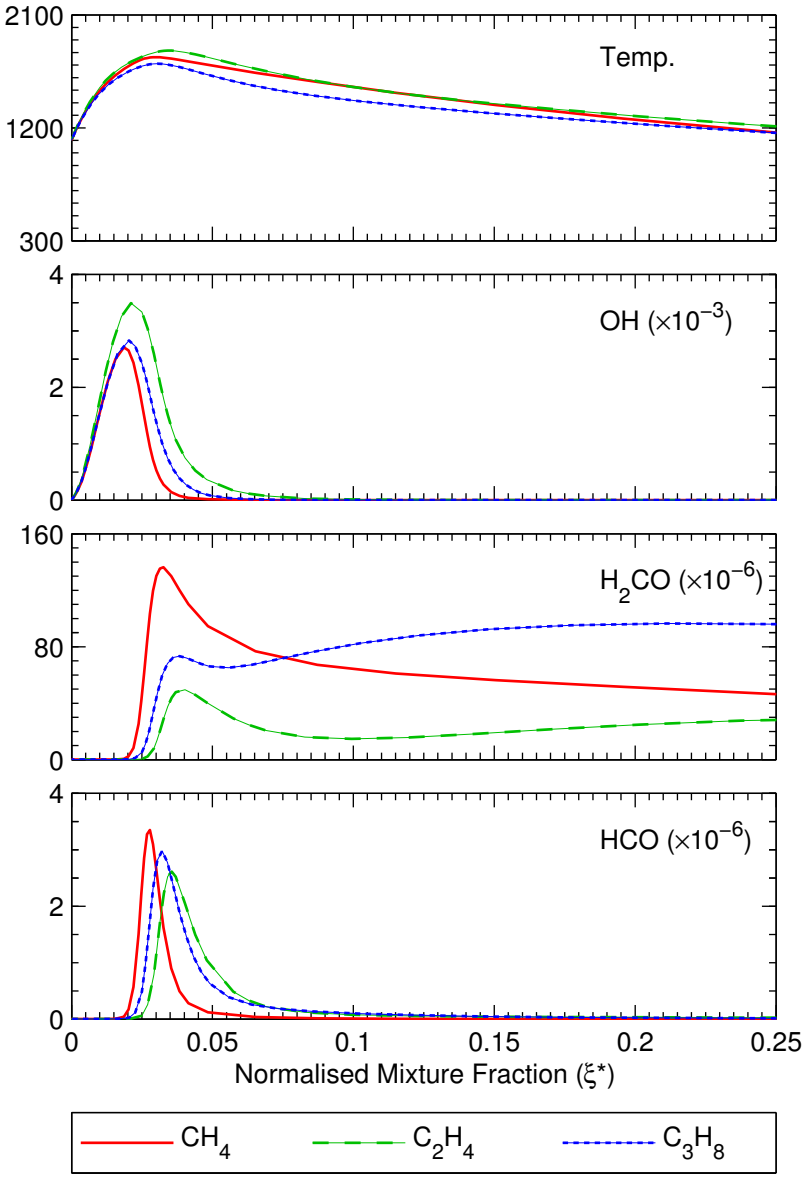

Fig. 8. Temperature and species mole fractions from strained laminar flame calculations in (normalised) mixture fraction space for 9% O_2 coflow composition ($a \approx 100 s^{-1}$).